Journal of
*Marine Science and Engineering*

*Article*

# Wind Speed Analysis Method within WRF-ARW Tropical Cyclone Modeling

**Evgeny Poplavsky [1], Alexandra Kuznetsova [1,2,*] and Yuliya Troitskaya [1]**

[1] Federal Research Center A.V. Gaponov-Grekhov Institute of Applied Physics of the Russian Academy of Sciences (IAP RAS), 603950 Nizhny Novgorod, Russia; poplavsky@ipfran.ru (E.P.); yuliya@ipfran.ru (Y.T.)
[2] Moscow Center for Fundamental and Applied Mathematics, 119991 Moscow, Russia
* Correspondence: alexandra@ipfran.ru

**Abstract:** This paper presents an analysis of a new method for retrieving the parameters of the atmospheric boundary layer in hurricanes. This method is based on the approximation of the upper parabolic part of the wind speed profile and the retrieval of the lower logarithmic part. Based on the logarithmic part, the friction velocity, near-surface wind speed and the aerodynamic drag coefficient are obtained. The obtained data are used for the verification of the modeling data in the WRF-ARW model. The case of the Irma hurricane is studied. Different configurations of the model are tested, which differ in the use of physical parameterizations. The difference of wind profiles in various sectors of the hurricane is studied.

**Keywords:** hurricane wind speeds; atmospheric model; WRF; GPS-dropsondes; wind speed profiles; verification

check for updates

**Citation:** Poplavsky, E.; Kuznetsova, A.; Troitskaya, Y. Wind Speed Analysis Method within WRF-ARW Tropical Cyclone Modeling. *J. Mar. Sci. Eng.* **2023**, *11*, 1239. https://doi.org/10.3390/jmse11061239

Received: 28 April 2023
Revised: 13 June 2023
Accepted: 14 June 2023
Published: 16 June 2023



## 1. Introduction

Tropical cyclones are currently one of the most dangerous weather phenomena, often leading to the loss of human lives and causing great damage to industry and transport [1]. They are observed predominantly in the tropics but can have a significant impact on the weather of temperate and subtropical zones due to the extratropical transition of TC [2,3], which is accompanied by high wind speeds and heavy rainfall, causing flooding both in coastal areas and the mainland. In this regard, the forecasting and monitoring of such phenomena, for example, the correct assessment of wind strength, are of practical value.

The microwave method of satellite remote sensing is one of the most important methods for determining the surface wind speed over the sea for monitoring weather conditions in the presence of clouds and precipitation. Such conditions are typical for storms but they do not strongly affect microwave electromagnetic waves. The near-surface wind speed is retrieved using empirical geophysical model functions (GMF). This relates the characteristics of the radiation scattered by the sea surface and the wind speed [4–6]. To build the GMF, along with satellite data, field measurements are also needed. The data from buoys and from GPS-dropsondes dropped over hurricanes are used.

The analyzed GPS-dropsondes are launched from National Oceanic and Atmospheric Administration (NOAA) and United States Air Force (USAF) aircraft reconnaissance missions into tropical cyclones in the Atlantic and Eastern Pacific basins in order to collect up-to-date information on environmental parameters in extreme conditions [7]. Most of such research has traditionally been conducted to assess Category 5 and Category 4 hurricanes on the Saffir–Simpson scale, which have the most damaging environmental impacts. The selected dataset for analysis and processing is from the NOAA Hurricane Research website [8].

NOAA GPS-dropsondes are widely used to measure wind speed in tropical cyclones at a height of 10 m. The main problem in determining surface wind speed in extreme storm conditions is large measurement errors near the surface, mainly for GPS-dropsondes.

In [9], one of the approaches is used to estimate such wind speeds within the lower 150 m layer of the atmosphere. The essence of this approach is that the average wind speed in the lower 150 m layer of the atmosphere is calculated, and the 10 m wind speed is recalculated by multiplying the obtained average value by 0.85. In [10], the WL150 algorithm is evaluated for SFMR winds. It shows that wind averaging over thinner layers, in particular, 100 m, 50 m, and especially 25 m, has lower biases and is more suitable for retrieving 10 m wind speed. Thus, the methods used to determine the wind speed using GPS-dropsondes at a height of 10 m require further study. In [11], the authors proposed a method for processing data from GPS-dropsondes that makes it possible to determine the parameters of the atmospheric boundary layer. It includes the near-surface wind speed, which is obtained from measurements in the upper part of the atmospheric boundary layer, excluding the use of the WL150 algorithm or direct measurements of the 10 m wind from GPS-dropsondes, where the data are characterized by a large scatter and errors. In addition, at a sufficient distance from the water surface (usually two or three significant wave heights), the momentum flux from the wind to the waves, which causes a deformation of the velocity profile, disappears (see, for example, [12]). Within the framework of this approach, the air flow velocity profiles averaged over turbulent fluctuations are used to obtain geophysical parameters. The advantage of this method is that each hurricane is considered separately and uses a much smaller set of GPS-dropsonde data for averaging. This method also allows one to retrieve the wind friction velocity associated with turbulent stress directly, in addition to wind speed. Tangential turbulent stress characterizes the tangential force of the wind on the water surface and determines the energy flow to the waves, the mixing in the upper layer of the ocean. It is the driving force of ocean circulation.

The developed wind speed retrieval methods are applied for comparison with the calculations of the atmospheric model for the case of a hurricane. Atmospheric parameters were determined using the Weather Research and Forecasting, WRF-ARW (WRF), atmospheric model [13]. The WRF is suitable for use in a broad range of applications, including parameterization research, polar research [14] and hurricane research. The hurricane numerical simulation quality is determined from the accuracy of the prediction of its trajectory and intensity. The results of the calculation are largely determined by the use of a set of parameterizations of physical processes included in the calculation. Thus, in this paper, we analyze approaches to modeling hurricanes in the WRF atmospheric model using certain parameterizations. A comparison of the performed calculations with the data of the GPS-dropsondes will make it possible to analyze the wind velocity profiles in a hurricane.

## 2. Methods

### 2.1. Study Object

Hurricane Irma was chosen for the research carried out in this work. This is a very powerful and destructive Cape Verde-type hurricane that developed during the period 30 August 2017–12 September 2017 in the Atlantic Ocean. Irma was assigned Category 5 on the Saffir–Simpson scale on 5 September 2017. Hurricane Irma is indicative and convenient for analysis; in addition, various data on atmospheric parameters have been published on it [15].

### 2.2. Data Preparation in the WRF Preprocessing System (WPS)

Data preparation for hurricane modeling was carried out in the WRF Preprocessing System (WPS). Geographical data "modis_lakes" were used for calculations. Nested domain simulations were carried out. Test simulations for the analysis of the used parameterizations were carried out for three nested domains, and for the final comparison of wind speed profiles, simulations for four nested domains in the hurricane passage area were carried out. The cell size of the third nested domain is ~3.3 km; the fourth was ~1.1 km (Figure 1). These data were used to describe the domains and to interpolate static geographic information to given grids. To describe the current meteorological situation, meteorological data from "Climate Forecast System Reanalysis Version 2 (CFSv2) (ds094.0)" [16] were used. It was updated every 6 h. Next, the extracted meteorological data were horizontally interpolated onto domain grids. The start date of WRF simulations was 9 May 2017 06:00 UTC.

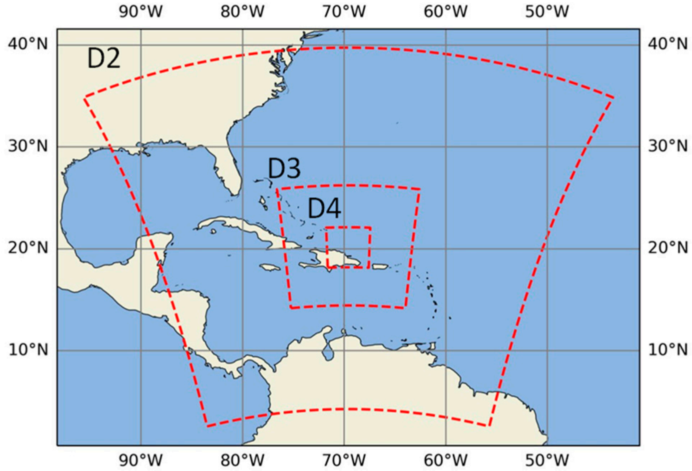


**Figure 1.** Location of nested domains (D2, D3, D4) in WRF atmospheric model simulations.

### *2.3. Modeling within WRF*

The hurricane was simulated using the atmospheric WRF model version 4.3.1. This model consists of 48 terrain-following sigma-pressure coordinates in the vertical direction, with the top layer kept at 50 hPa. The simulations were carried out for 90 h, including 12 h of spin-off time. The simulation was performed in the MPI option on the IAP RAS cluster. The resulting data were obtained with a time step of 1 h.

Parameterization schemes represent the physical processes that are unresolved by the WRF model. Following the recommendations of the authors of the model [13], a set of parameterizations for the case of a hurricane (configuration #2 in Table 1) was initially used in the calculations, which consisted of a parameterization of microphysics option WRF Single-moment 6-class Scheme [17], shortwave and longwave radiation option RRTMG Scheme [18], a surface layer of the atmosphere option Revised MM5 Scheme [19], a planetary boundary layer option Yonsei University Scheme (YSU) [20], and a cumulus parameterization option Tiedtke Scheme [21]. At the same time, to describe the land surface model, the parameterization of the 5-layer Thermal Diffusion Scheme [22] was used. This configuration was expected to best describe the track and intensity of the hurricane. However, calculations with such a set of parameterizations showed too much deviation of the hurricane's trajectory in comparison with satellite images and HURDAT2 dataset (see Table 2). Therefore, an analysis of the sensitivity of the model to the use of different parameterizations and an assessment of the impact of their use on the trajectory of the hurricane, its shape and intensity was conducted. More than 35 numerical experiments were carried out with different sets of parameterizations. Some cases are shown in Table 1. The parameterizations shown were chosen because they are the most widely used schemes for regional climate modeling in WRF.

The main interest was the choice of parameterization of the atmospheric parameters, particularly the planetary boundary layer (PBL) parameterization. The existing PBL parameterizations mostly describe the convective boundary layer under low-wind conditions and poorly predict such high wind speeds that occur in tropical cyclones [23]. In such parameterizations, turbulence is predominantly buoyancy-driven, whereas in the hurricane's boundary layer turbulence is predominantly shear-driven. Buoyancy becomes more important in the upper boundary layer when vertical wind shear gets weaker. Nevertheless, these schemes of PBL are widely used to predict hurricane events, but the performance of such models needs to be controlled [24]. In this study, two first-order PBL schemes with nonlocal closures are considered. One of them is YSU [20], it is a widely used scheme in WRF to the hurricane simulations. Another one is the NCEP Global Forecast System Scheme (GFS) [25], it is used in the operational HWRF model [26], specifically designed for tropical cyclone applications. On the other hand, the Mellor–Yamada–Nakanishi–Niino Level 2.5 (MYNN) scheme [27,28] is a 1.5-order local closure scheme based on a prognostic equation for turbulent kinetic energy. The MYNN scheme does not fully account for deeper vertical mixing induced by large eddies but has a higher-order closure. In addition, another approach is tested in this study: the application of large eddy simulation (LES) is tested in the last domain. The use of LES resolves individual eddies. The LES option [29] is recommended for use at a spatial resolution of the domain step of less than 1 km; however, its use is also acceptable and studied at a lower spatial resolution [30,31]. The Kessler Scheme [32] and WRF Single-moment 6-class Scheme schemes were used as microphysics options, and the Kain–Fritsch Scheme [33] and Tiedtke Scheme were used as cumulus parameterizations. The Kain–Fritsch Scheme has more active shallow convection over the ocean surface than the Tiedtke Scheme, and it was interesting to compare these two approaches. The 5-layer Thermal Diffusion Scheme approach was used to describe the underlying surface. Together with GFS PBL and the surface layer, the Unified NOAH Land Surface model [34] was used. The CAM Shortwave and Longwave Radiation Scheme [35] and RRTMG Shortwave and Longwave Radiation Scheme were used to describe shortwave and longwave radiation. Numerical experiments with the use of the ocean model [36] and with the use of modified surface bulk drag in surface layer parameterization using the Donelan formulation [37] were also carried out.

**Table 1.** Set of parameterizations in various configurations of WRF simulations.

| # | PBL Physics | Surface Layer | Micro Physics Options | Cumulus Parameterization | Shortwave and Longwave Radiation | Special Options |
|---|---|---|---|---|---|---|
| 1 | YSU | Revised MM5 | Kessler Scheme | Kain–Fritsch | CAM | n/a |
| 2 | YSU | Revised MM5 | WRF Single–moment 6–class | Tiedtke | RRTMG | "hurricane case" |
| 3 | MYNN | MYNN | WRF Single–moment 6–class | Kain–Fritsch | RRTMG | n/a |
| 4 | YSU + LES | Revised MM5 | Kessler Scheme | Kain–Fritsch | RRTMG | LES |
| 5 | YSU | Revised MM5 | WRF Single–moment 6–class | Kain–Fritsch | RRTMG | n/a |
| 6 | YSU | Revised MM5 | WRF Single–moment 6–class | Kain–Fritsch | RRTMG | OCEAN1 coupling |
| 7 | YSU + LES | Revised MM5 | Kessler Scheme | Kain–Fritsch | RRTMG | LES; drag coefficient by Donelan |
| 8 | GFS | GFS | Kessler Scheme | Kain–Fritsch | RRTMG | HWRF atmospheric components |

**Table 2.** Average deviation between the predicted trajectory and track from the HURDAT2 dataset for each configuration.

| Configuration # | 1 | 2 | 3 | 4 | 5 | 6 | 7 | 8 |
|---|---|---|---|---|---|---|---|---|
| Average deviation, km | 138.18 | 98.27 | 72.96 | 130.25 | 74.35 | 93.7 | 106.42 | 88.02 |

### *2.4. Data Processing of GPS-Dropsondes*

In this paper, an analysis of a new method for retrieving the parameters of the atmospheric boundary layer in hurricanes is presented. The method is based on the self-similarity of the wind velocity profile in the boundary layer [38], which is well-described by the empirical function

$$U_{\max} - U(z) = \begin{cases} u_* \left( -\frac{1}{k} \ln(z/\delta) + \gamma \right); z/\delta < 0.3, \\ \beta u_* (1 - z/\delta)^2; z/\delta > 0.3. \end{cases} \tag{1}$$

where $U_{\max}$ is the maximum speed in the atmospheric boundary layer, $k = 0.4$ is the von Kármán constant, $\delta$ is the boundary layer thickness and $u_*$ is friction velocity.

A similar method was used in laboratory experiments [12] and is suitable for retrieving parameters in tropical cyclones. The profiles averaged over the statistical ensembles and the profiles of the simulated hurricane are similar to the wind velocity profiles measured under laboratory conditions in the wind wave channel. They have a logarithmic slope in the lower part of the profile and a parabolic portion in the upper part, where the boundary layer passes into the external flow. The upper lid restricting the flow of air masses is the capping inversion of the atmosphere. This similarity makes it possible to use our modified profiling method to retrieve the dynamic parameters of the boundary layer, which was previously successfully applied in laboratory facilities. The essence of this method is that, by approximating the upper parabolic part of the wind speed profile, one can retrieve the lower logarithmic part and obtain boundary layer parameters that are important for numerical weather models, such as friction velocity, near-surface wind speed, and aerodynamic drag coefficient. This approach avoids the use of measurements near the surface, where the data are characterized by a large scatter and errors. In addition, at a sufficient distance from the water surface (usually 2–3 significant wave heights), the momentum flux from the wind to the waves disappears, which causes a deformation of the velocity profile [12]. The parameters $U_{\max}, u_*, \delta$ included in Formula (1) can be obtained using the second-degree polynomial approximation of the measured velocity profile in the "trace" part, i.e., at $z/\delta > 0.3$:

$$U(z) = p_3 + p_2 z + p_1 z^2. \tag{2}$$

Comparison with (1) yields relationships that allow one to calculate the parameters of the turbulent boundary layer $U_{\max}, u_*, \delta$:

$$\beta u_* = -\frac{p_2^2}{4p_1}; \delta = -\frac{p_2}{2p_1}; U_{\max} = p_3 + \beta u_*. \tag{3}$$

Constants $\gamma$ and $\beta$ were obtained by approximating the experimental data using Formula (1) [see. 12]: $-1/(k\beta) = 0.3474 \pm 0.014$ and $\gamma/\beta = 0.07318$. Then, using (3), the friction velocity can be calculated and, using the obtained values $U_{\max}, u_*, \delta$, the roughness parameter, 10 m wind speed $U_{10}$ and the aerodynamic drag coefficient can be calculated:

$$\begin{gathered} z_0 = \delta \exp(-kU_{\max}/u_* + \gamma k) \\ U_{10} = \frac{u_*}{k} \ln(H_{10}/z_0) \\ C_D = \left( \frac{u_*}{U_{10}} \right)^2 = \frac{k^2}{(kU_{\max}/u_* - \gamma k + \ln(H_{10}/\delta))^2}, \end{gathered} \tag{4}$$

where $H_{10} = 10$ m.

It should be noted that self-similar laws for velocity profiles in a turbulent boundary layer are applicable only to values averaged over a statistical ensemble. Such ensembles are groups of wind velocity profiles measured at of the order of equal distances from the hurricane center [39]. In Figure 2a, an example of an averaged profile and a parabolic approximation of the upper part of the atmospheric boundary layer can be seen. This method works for the majority of the average wind speed profiles obtained in a hurricane. Nevertheless, profiles similar to the profile in Figure 2b arise. In the lower logarithmic part, the profile has two segments with different slopes. This complicates the data processing and leads to an incorrect determination of the wind speed $U_{10}$ and other parameters. This can be explained by the fact that the GPS-dropsonde does not fall straight down, but deviates during the fall and enters the zones of the hurricane of different intensity. The difficulties faced in the processing of data from GPS-dropsondes motivated us to perform hurricane simulations in order to analyze the behavior of velocity profiles in it.

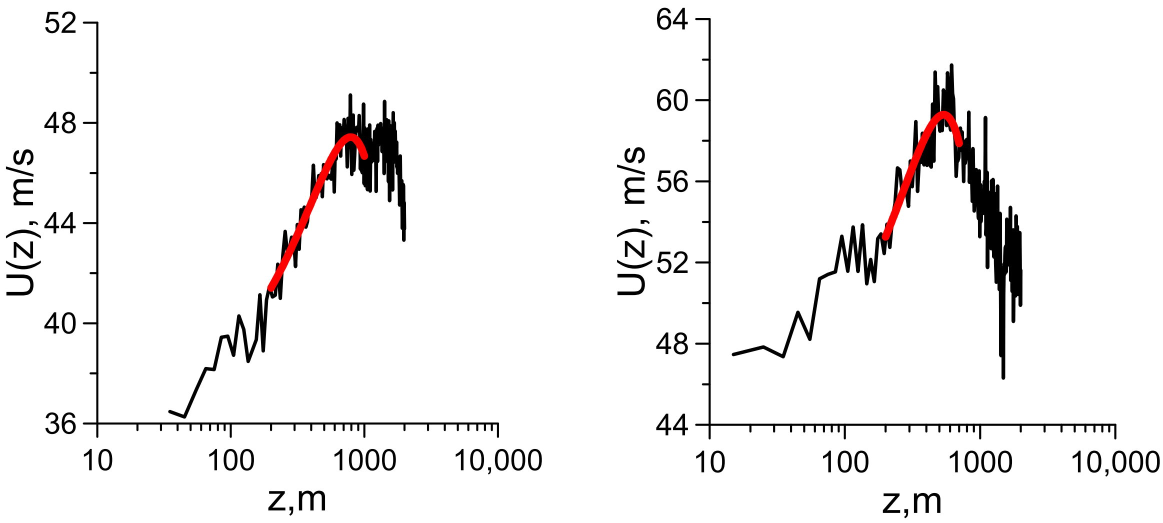


(**a**) (**b**)

**Figure 2.** (**a**) Averaged profile from GPS-dropsondes dropped at a distance of (**a**) 100–110 km from the center of the hurricane (Irma, 2017) and (**b**) 40–45 km from the center of the hurricane (Rita, 2005).

## 3. Results and Discussion

The results of the WRF model simulations were obtained using model configurations that differ in the use of various physical parameterizations (examples are shown in Table 1). All the configurations tested showed a significant deviation in the hurricane's track (Figure 3). In Figure 3, the wind speed distribution at 18:00 on 9 July 2017 from the WRF simulation with configuration #5 (see Table 1) is shown.

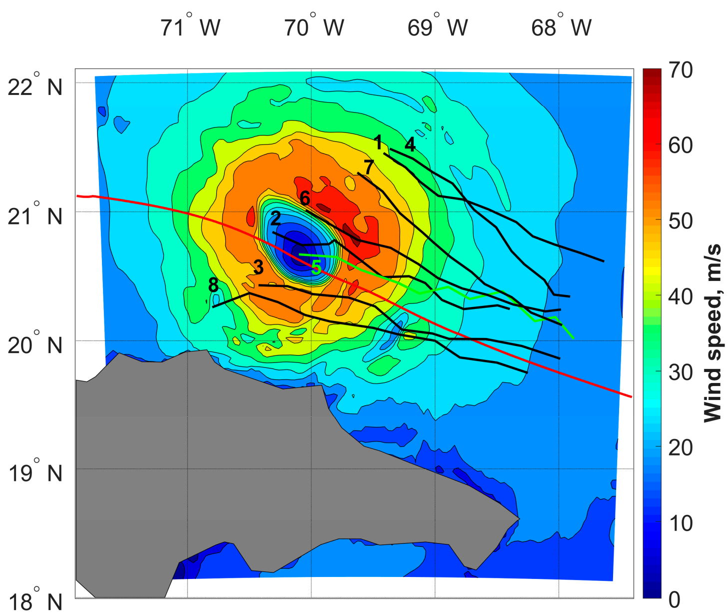


**Figure 3.** Wind speed distribution (m/s) (9 July 2017 18:00) obtained from WRF simulations. The red line is the track of Hurricane Irma according to [15]. The green line is the hurricane track obtained from the simulation results with configuration #5 (see Table 1). Black lines are hurricane tracks obtained with other configurations (the number corresponds to Table 1).

In Table 2, the average deviation of the track is demonstrated. It was defined as a mathematical average of the distance between the modeled track and HURDAT2 dataset trajectory. The problem of hurricane trajectory deflection during modeling is known and described, for example, in [40].

Configuration #1 demonstrates a significant deviation of the hurricane track from the HURDAT2 dataset; in addition, the size of the hurricane is significantly overestimated (by 30%) compared to satellite imagery data from Sentinel-1. The wind speed distribution in Figure 4a is obtained from the remote sensing data using GMF from [41]. However, the use of this configuration provides a stable structure of the hurricane and the wind speed profiles have the expected logarithmic slope at high wind speeds. Replacing the option of shortwave and longwave radiation with RRTMG significantly reduces the deviation of the calculated track from the one observed. With the same scheme for describing shortwave and longwave radiation, configuration #2 is tested. The set of parameterizations in this configuration corresponds to the "hurricane case" specified in the recommendations of [13] for hurricane wind conditions. The track of the calculated hurricane in this case is close to the observed one, but the size of the eyewall is highly overestimated (by two times) and varies in structure along its path.

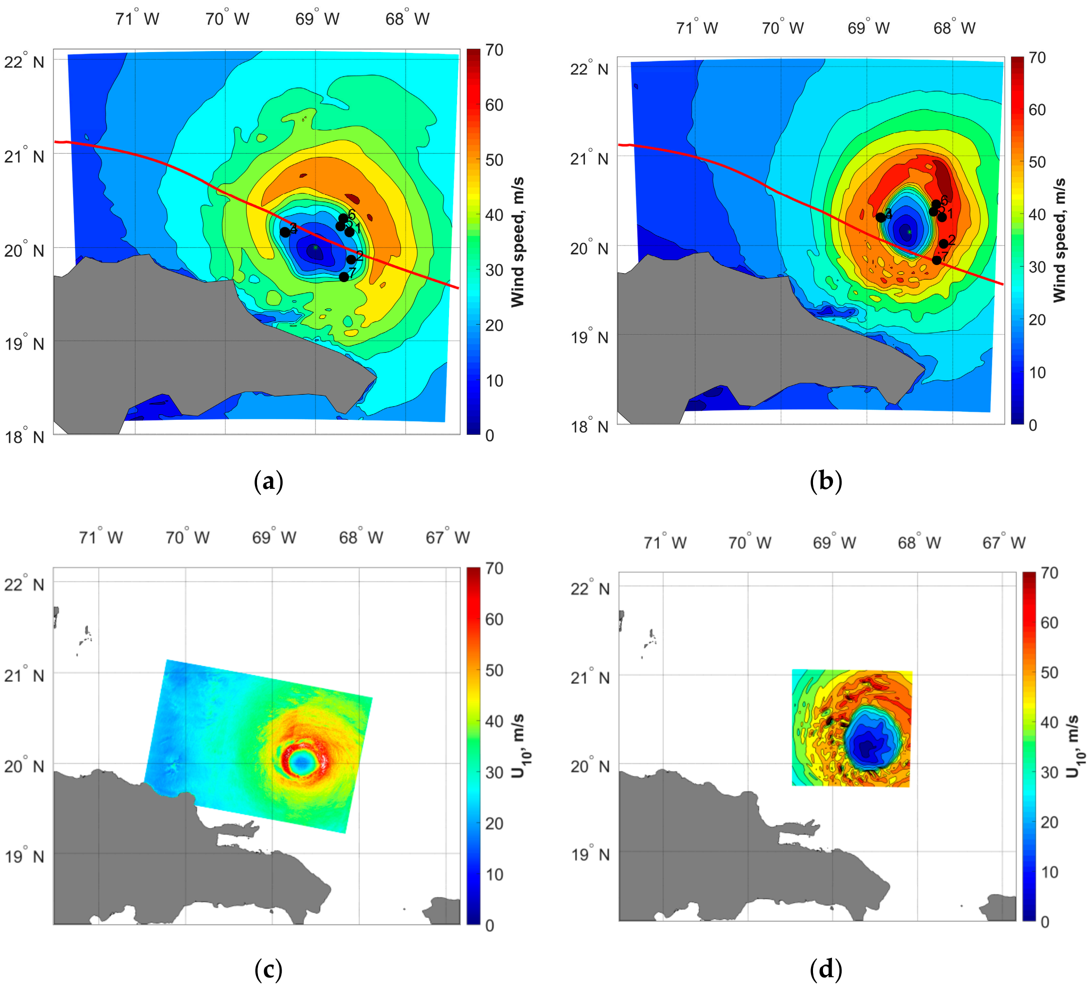


**Figure 4.** Wind speed distribution (m/s) (9 July 2017 11:00) obtained from (**a**) WRF simulations, configuration #8, domain 3; (**b**) WRF simulations, configuration #5, domain 3; (**c**) remote sensing data Sentinel-1 using GMF from [41]; and (**d**) WRF simulations, configuration #5, domain 4 (Table 1).

In configuration #3, the use of a different parameterization of the PBL and the surface layer of the atmosphere, MYNN, is tested. This configuration demonstrates a slight deviation from the HURDAT2 dataset track, and this result is promising in terms of the further study of the influence of PBL parameterizations. Another possibility to improve the PBL description is coupling with wave models due to the improvement in the drag coefficient parameterizations in the atmospheric models. Unfortunately, for the moment, in the results when using this configuration, the size of the eyewall is overestimated compared to satellite imagery data and it has a highly variable structure throughout its movement.

In configuration #4, the large eddy simulation (LES) approach is used. In this method, the track is strongly deviated and the size of the hurricane is overestimated by 150%; the structure of the hurricane is also unstable. Among the considered approaches, the best agreement with the measurement results was obtained using configuration #5. In this case, the same set of parameterizations is used as in configuration #2, except for the cumulus parameterization: the Kain–Fritsch scheme was used instead of the Tiedtke scheme. The track of the hurricane is close to the observed one, and the size of the eyewall better corresponds to the data of satellite images. In Figure 4d, the wind speed distribution in the fourth domain at 11:00 on 9 July 2017 from the WRF simulation with configuration #5 is shown. This point in time corresponds to the moment of the Sentinel-1 imagery data (as in Figure 4c). Wind speed profiles have a logarithmic slope.

The use of coupled modeling with the ocean model was also tested: configuration #6 differs from configuration #5 only in that it takes into account the ocean model. However, the track deviation in this case turns out to be larger. The simulation using LES in configuration #7 also turned out to be unsatisfactory. The track of the simulated hurricane in this case is very different from the observed one, and the eye of the hurricane is highly overestimated.

Configuration #8 has a set of atmospheric parameterizations similar to the HWRF operational model [26]. This configuration also provides a satisfactory deviation of the hurricane trajectory. In Figure 4a,b, the resulting wind speed distributions in the 3d domain are compared using configurations #8 and #5. In configuration #8, the size of the eyewall is a bit overestimated. This causes dropsondes to fall inside the eye of the hurricane, which is inconsistent with observations. It should be noted that the HWRF modeling is not used in this configuration, only HWRF atmospheric components (PBL, surface layer parameterizations). The HWRF is designed specifically for hurricane forecasting, allowing vortex tracking during the integration period. The use of the complete HWRF approach will lead to better trajectory and intensity prediction [26]. However, at the moment, WRF simulations within configuration #5 are used for further comparison with the dropsonde data.

For comparison, the GPS-dropsondes dropped at approximately equal distances from the center of the hurricane (scatter 5–10 km) [39] were selected. The obtained data on wind speed profiles were averaged. The averaged profiles of the GPS-dropsondes of the WRF simulation were obtained at the same distance from the center of the hurricane. For the averaging, the profiles that are located in the coordinates of the fall of the dropsondes were used. The wind speed distribution from the WRF simulation (Figure 5a,c,e,g) is shown at 14:00 on 9 July 2017 to let all the considered locations of the dropsondes fit the domain. The center of the hurricane was determined from the results of the simulation. It was calculated as the center of the circle obtained for a wind speed value of 50 m/s, since the track of the simulated hurricane does not coincide completely with the remote-sensing data.

The averaged profile of the dropsondes located at a distance of 40–50 km from the center (Figure 5b) shows slightly higher wind speeds than the profile obtained from the simulation results.

The averaged profile of the next set of dropsondes (70–80 km from the center of the hurricane "eye", Figure 5d) shows a lower wind speed than the simulated one. At distances of 100–110 km (Figure 5e) and 150–160 km (Figure 5h), the profiles behave similarly and almost coincide. Perhaps the behavior of the averaged wind speed profiles is due to the fact that the size of the eye of an observed hurricane and that of the simulated one are slightly different, and this difference is the most pronounced in the region of the wall of the "eye" of the hurricane, since the highest wind speeds are observed there. It is also worth noting that the simulated wind speed profiles have a pronounced logarithmic slope in the lower part at high wind speeds, just like the profiles from the dropsondes.

The use of the data in the third domain proves to be convenient for observing the dynamics of a hurricane and testing different sets of parameterizations for its simulation. For a more detailed study of hurricanes, simulations with this configuration for four nested domains with a resolution of 1 km in the last domain were performed. The location of the fourth domain was chosen taking into account the resulting track of the simulated hurricane in the third domain, since the fourth domain has a slightly larger size than the hurricane itself, and it is necessary to match its position. The modified profiling method used in [31] and partially presented in Section 2.4 is based on the self-similarity of wind velocity profiles in a hurricane, and it is assumed that it is the same for the entire hurricane. Using the obtained simulation results, it is interesting to analyze how the self-similarity process is carried out and whether it is the same in different sectors of the hurricane.

Similar to the algorithm described in Section 2.4, to obtain constants $\gamma$ and $\beta$, it is necessary to plot the wind speed profiles obtained as a result of the calculation in dimensionless variables. However, in the case of GPS-dropsondes, each profile is considered separately. It is not possible for the simulated data since the amount of data is many times greater than the experimental ones. To achieve this, automatic sorting of the simulated wind speed profiles was carried out, which have a positive logarithmic slope in the lower part of the profile, since the profiles located in the zone of low wind speeds (the "eye" of the hurricane or at a great distance from its center) are vertical or tilted in the opposite direction and are not suitable for profiling. In Figure 6, all used wind speed profiles in self-similar variables are shown.

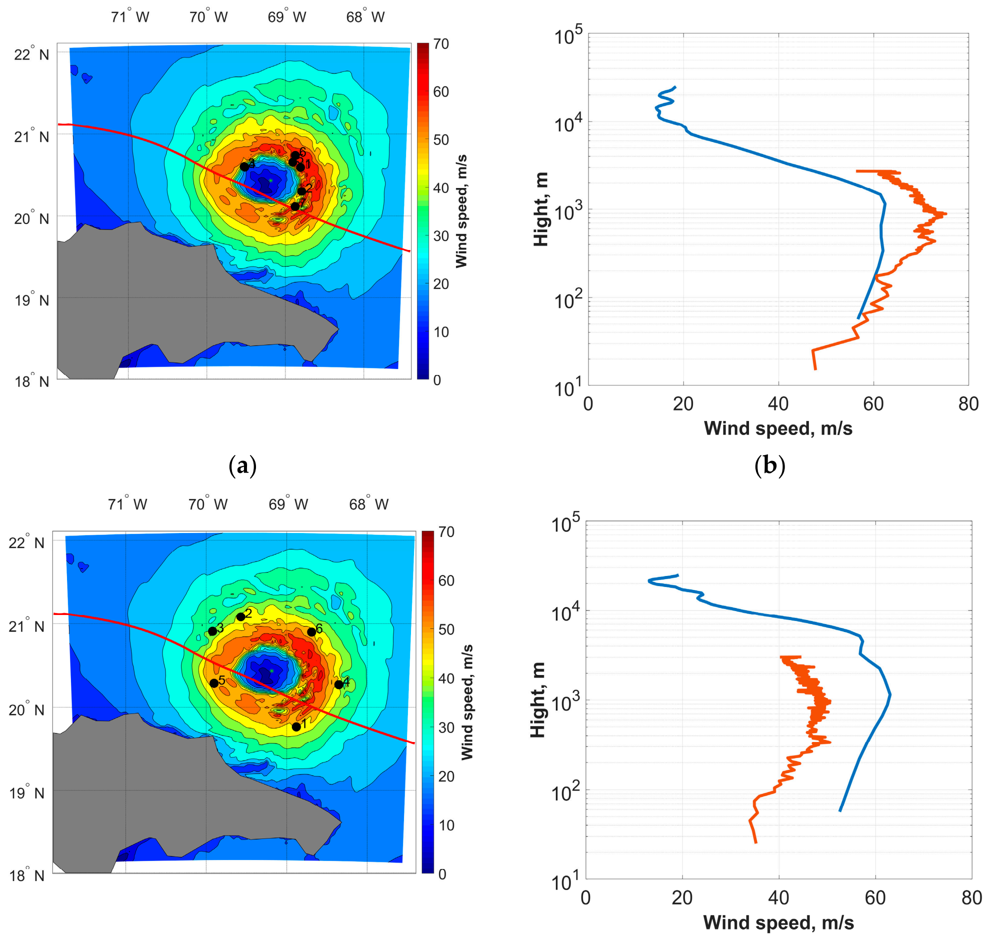


(**a**) (**b**) (**c**) (**d**)

**Figure 5.** *Cont.*

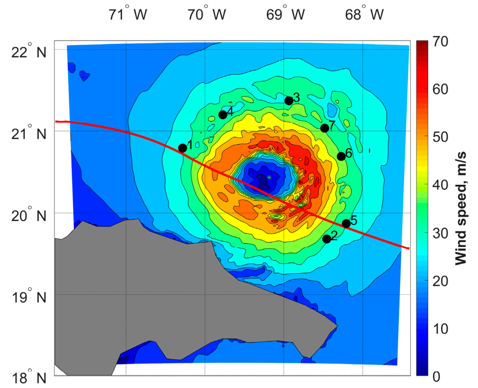


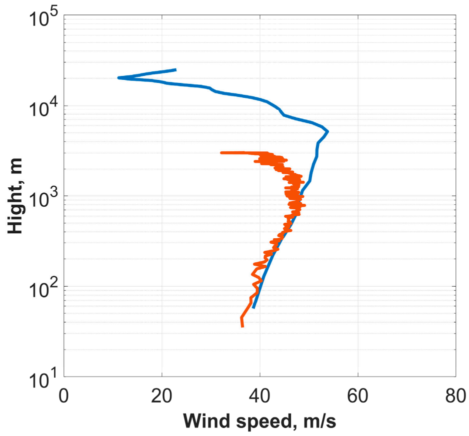


(**e**) (**f**)

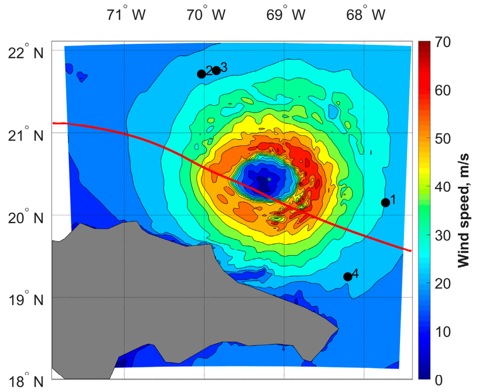


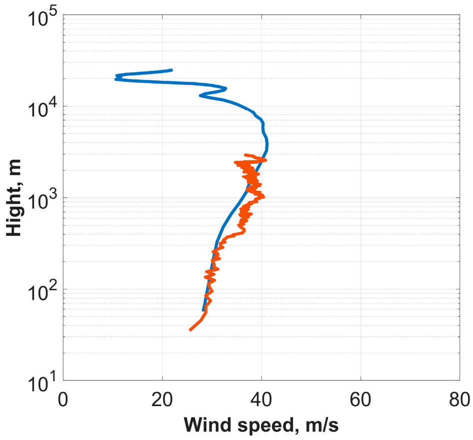


(**g**) (**h**)

**Figure 5.** Distribution of 10 m wind speed (**a**,**c**,**e**,**g**) m/s (9 July 2017 14:00) and comparison of the averaged vertical wind speed profiles of the hurricane obtained as a result of WRF simulations and GPS-dropsondes (**b**,**d**,**f**,**h**). The black points on the left show the coordinates of the fall of the GPS-dropsondes; the red curve is the observed track of the hurricane. On the right, the orange wind speed profile is the averaged profile of the group of GPS-dropsondes and the blue one is the averaged profile of the simulated hurricane at the same coordinates. Distance to the center of the hurricane: 40–50 km (**b**), 70–80 km (**d**), 100–110 km (**f**), 150–160 km (**h**).

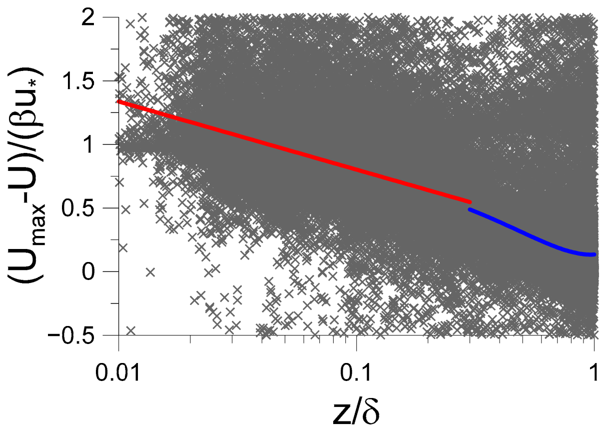


**Figure 6.** Wind speed profiles from the hurricane Irma simulations in self-similar variables. The red line is the logarithmic approximation of the lower part of the boundary layer ($z$/delta < 0.3); the blue one is the polynomial approximation ($z$/delta > 0.3).

As can be seen in Figure 6, the profiles are indeed grouped with a certain spread around one curve, which consists of a logarithmic part and a parabolic part.

In [42], three sectors are distinguished in hurricanes based on the observation of different waves in them. It should be assumed that the form of self-similar dependences in different parts of the hurricane may also differ. Using the same division of the hurricane into three sectors, one can build separate self-similar dependencies for each of them and compare the obtained coefficients (or, in fact, the slopes of the logarithmic part). The division of the hurricane into sectors was carried out as follows (Figure 7): from the direction of the hurricane's movement, the first sector lay in the area of 20–150 degrees; the second—150–240 degrees; and the remaining area is the third sector.

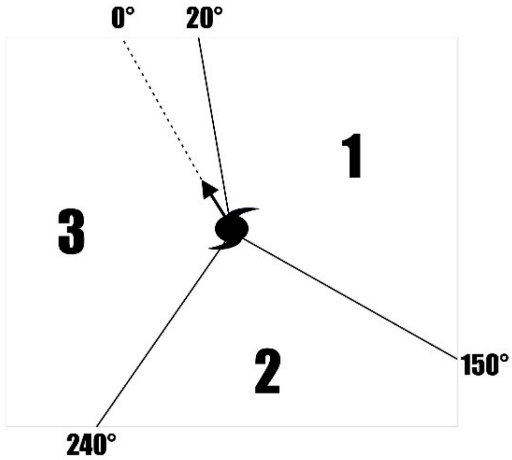


**Figure 7.** Sector division of the hurricane according to [34]; the arrow indicates the direction of the hurricane's motion.

As a result, the following values for the coefficient were obtained: 10.09 +/− 0.225 (sector 1), 9.80 +/− 0.35 (sector 2), and 12.89 +/− 0.46 (sector 3) (Figure 8). As can be seen from these values, the coefficient for the third sector is allocated, while the coefficients for the first and second sectors are approximately the same within the confidence intervals.

To investigate the behavior of these sectoral self-similar dependences on distance, the data are split into bins of 10 km by distance from the center of the hurricane, starting from 40 km, where the eye wall of the hurricane with high wind speeds begins. On Figure 9 the obtained results are shown, namely, the dependence of the coefficient on the distance to the center of the hurricane for each sector. The dependences for the first and second sectors behave similarly in almost the entire area under study, except for the range of 62.5–67.5 km, where there is a slight difference between them. The dependence for the third sector differs quite significantly from the other two sectors outside the confidence intervals at distances from 47.5 km to 72.5 km. It should be noted that, in [42], the dependences of the aerodynamic drag coefficient on wind speed for these sectors are considered, and the dependence for the left-front sector also stand out noticeably from the rest, which is associated with the different waves in these sectors. Here, the difference in the coefficient $\beta$ may be due to the different behavior of the wind velocity profiles in the upper parabolic part of the atmospheric boundary layer. The wind in a tropical cyclone rotates in a spiral around its center counterclockwise in the Northern Hemisphere, and just in the left-front sector, the forward motion of the hurricane and the direction of the rotating winds are opposite, and it can be assumed that this has a large influence on the vortex structure of the atmospheric boundary layer for this sector, in contrast to the others. Due to different vortex structures, the wind speed profiles also differ, which, in turn, manifests itself in the difference in self-similar dependences. A similar situation is observed in [38], although for a turbulent flow in a pipe, where different coefficients are obtained for different vortex structures.

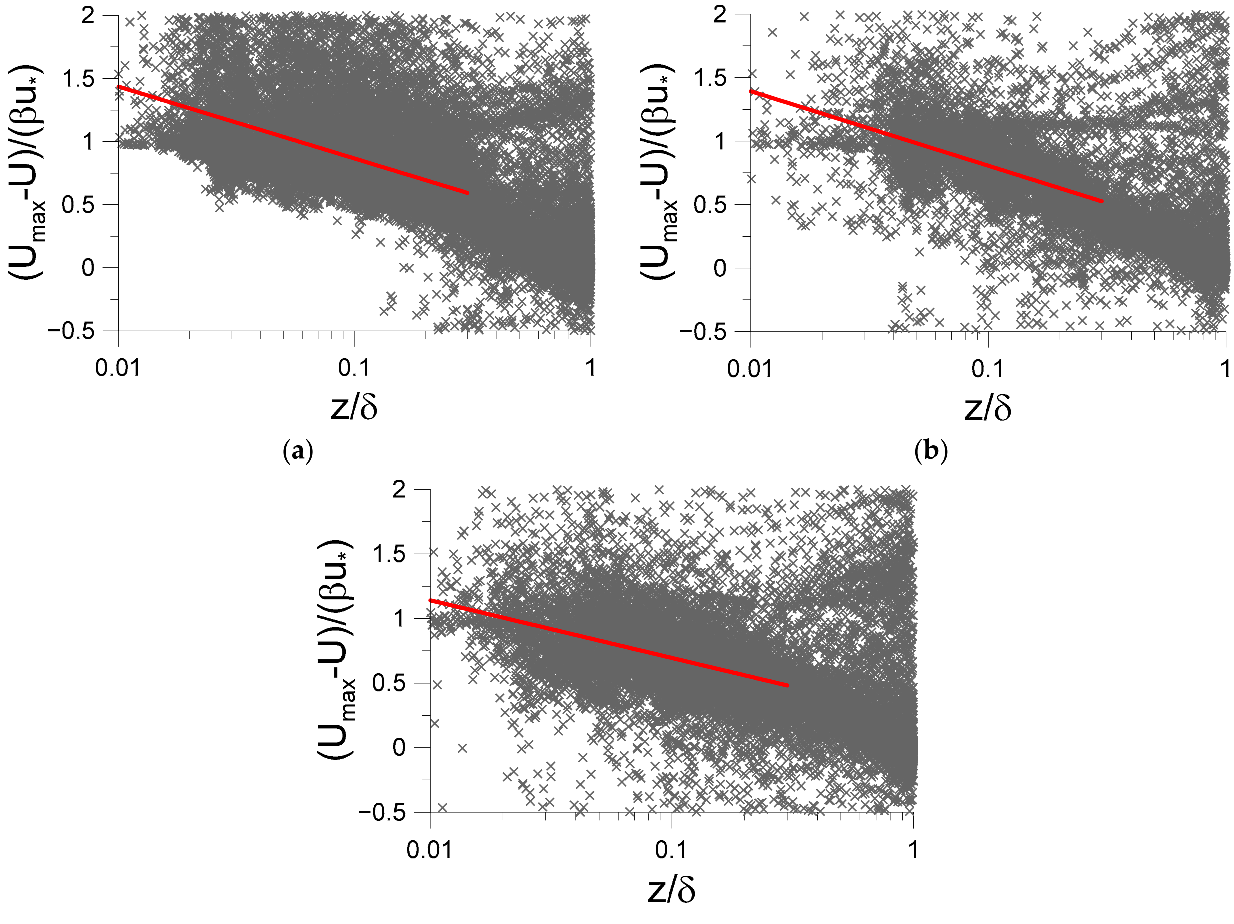


**Figure 8.** Self-similar wind speed profiles for sector 1 (**a**), sector 2 (**b**), and sector 3 (**c**). The red line is the logarithmic approximation of the lower part of the boundary layer (up to 0.3 $z/$delta).

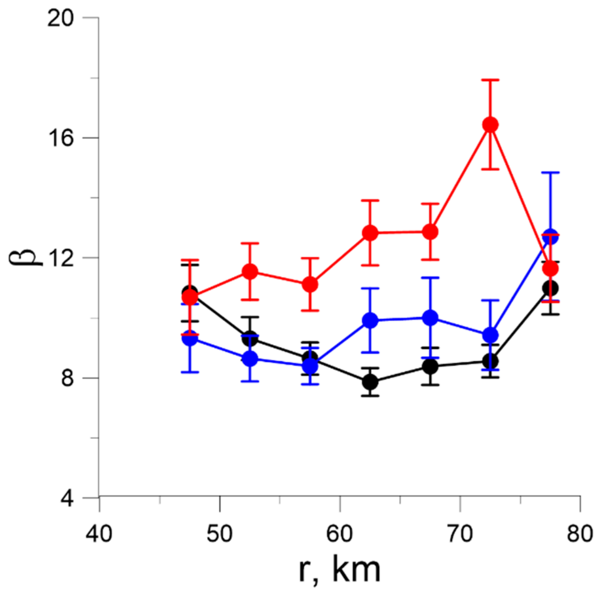


**Figure 9.** Dependence of the $\beta$ coefficient on the distance to the center of the hurricane for its three sectors. The black curve is for the 1st sector, the blue one is for the 2nd one, and the red one is for the 3rd one.

In previous works, the coefficients $\gamma$ and $\beta$ were obtained on the basis of a self-similar dependence built on the entire available data set from GPS-dropsondes without division into sectors. The estimation of the $\beta$ coefficients suggests that the self-similar laws differ slightly depending on the hurricane sector at certain distances to its center, and it would be useful to take this fact into account when reconstructing geophysical parameters, if there is a sufficient amount of experimental data.

## 4. Conclusions

In this paper, we have considered and analyzed a number of hurricane calculations with different sets of parameterizations. The configuration consisting of YSU parameterization for PBL, Revised MM5 as the surface layer option, WRF Single-moment 6-class for the microphysics option, the Kain–Fritsch scheme for cumulus parameterization and RRTMG as the shortwave and longwave radiation option was used for further analysis. The track of the simulated hurricane with this configuration shows a lower deviation of the track from the HURDAT2 dataset than other considered configurations simultaneously with the stable structure of the hurricane and its eyewall size coinciding with the remote sensing data from Sentinel-1. The wind speed profiles from GPS-dropsondes are in good agreement with the profiles obtained as a result of the calculation, and the size of its "eye" corresponds to satellite imagery.

The behavior of the self-similar dependences of wind velocity profiles in a hurricane, which are used to retrieve geophysical parameters, was studied, and it was found that the slope coefficient of the logarithmic part of these dependences slightly differs not only depending on the choice of the sector in the hurricane, but also on the distance to its center. The main obtained result suggests that when retrieving geophysical parameters, it would be useful to take into account the difference in self-similar dependencies in different sectors of the hurricane, if this allows the amount of data used for this reconstruction.

**Author Contributions:** Conceptualization, A.K. and Y.T.; methodology, A.K. and E.P.; software, A.K. and E.P.; validation, E.P.; writing—original draft preparation, A.K.; writing—review and editing, A.K.; visualization, E.P.; supervision, Y.T.; project administration, Y.T.; funding acquisition, A.K. and Y.T. All authors have read and agreed to the published version of the manuscript.

**Funding:** Alexandra Kuznetsova acknowledges President's grant MK-2489.2022.1.5 for the support of the WRF-ARW configuration analysis and coupling techniques. The WRF simulation was carried out with the financial support of the Ministry of Education and Science of the Russian Federation as part of the program of the Moscow Center for Fundamental and Applied Mathematics under the agreement No. 075-15-2022-284. Yuliya Troitskaya acknowledges the RSF grant #19-17-00209 for the support of the development of the wind speed analysis method. Evgeny Poplavsky acknowledges the RSF grant # 21-17-00214 (processing the GPS-dropsondes data).

**Institutional Review Board Statement:** Not applicable.

**Informed Consent Statement:** Not applicable.

**Data Availability Statement:** Data are available upon reasonable request.

**Conflicts of Interest:** The authors declare no conflict of interest.

## References

1. Needham, H.F.; Keim, B.D.; Sathiaraj, D. A review of tropical cyclone-generated storm surges: Global data sources, observations, and impacts. *Rev. Geophys.* **2015**, *53*, 545–591. [CrossRef]
2. Harr, P.A.; Elsberry, R.L. Extratropical Transition of Tropical Cyclones over the Western North Pacific. Part I: Evolution of Structural Characteristics during the Transition Process. *Mon. Weather. Rev.* **2000**, *128*, 2613–2633. [CrossRef]
3. Harr, P.A.; Elsberry, R.L.; Hogan, T.F. Extratropical transition of tropical cyclones over the western North Pacific. Part II: The impact of midlatitude circulation characteristics. *Mon. Weather. Rev.* **2000**, *128*, 2634–2653. [CrossRef]
4. Hersbach, H.; Stoffelen, A.; De Haan, S. An improved C-band scatterometer ocean geophysical model function: CMOD5. *J. Geophys. Res. Atmos.* **2007**, *112*, C03006. [CrossRef]
5. Hersbach, H. Comparison of C-Band Scatterometer CMOD5.N Equivalent Neutral Winds with ECMWF. *J. Atmos. Ocean. Technol.* **2010**, *27*, 721–736. [CrossRef]

6. Stoffelen, A.; Verspeek, J.A.; Vogelzang, J.; Verhoef, A. The CMOD7 Geophysical Model Function for ASCAT and ERS Wind Retrievals. *IEEE J. Sel. Top. Appl. Earth Obs. Remote. Sens.* **2017**, *10*, 2123–2134. [CrossRef]
7. Available online: https://www.nhc.noaa.gov/recon.php (accessed on 20 April 2023).
8. Available online: http://www.aoml.noaa.gov/hrd/data_sub/hurr.html (accessed on 17 November 2021).
9. Uhlhorn, E.W.; Black, P.G.; Franklin, J.L.; Goodberlet, M.; Carswell, J.; Goldstein, A.S. Hurricane Surface Wind Measurements from an Operational Stepped Frequency Microwave Radiometer. *Mon. Weather. Rev.* **2007**, *135*, 3070–3085. [CrossRef]
10. Polverari, F.; Sapp, J.W.; Portabella, M.; Stoffelen, A.; Jelenak, Z.; Chang, P.S. On Dropsonde Surface-Adjusted Winds and Their Use for the Stepped Frequency Microwave Radiometer Wind Speed Calibration. *IEEE Trans. Geosci. Remote. Sens.* **2022**, *60*, 1–8. [CrossRef]
11. Ermakova, O.S.; Sergeev, D.A.; Balandina, G.N.; Rusakov, N.S.; Poplavsky, E.I.; Troitskaya, Y.I. Institute of Applied Physics RAS Retrieval of atmospheric boundary layer parameters in a tropical cyclone from the data of falling GPS sondes. *Curr. Probl. Remote. Sens. Earth Space* **2019**, *16*, 301–309.
12. Kandaurov, A.A.; Troitskaya, Y.I.; Sergeev, D.A.; Vdovin, M.I.; Baidakov, G.A. Average velocity field in the air flow over the water surface in laboratory study of the hurricane conditions. *Izv. Atmos. Ocean. Phys.* **2014**, *50*, 399–410. [CrossRef]
13. Skamarock, W.C.; Klemp, J.B.; Dudhia, J.; Gill, D.O.; Liu, Z.; Berner, J.; Wang, W.; Powers, J.G.; Duda, M.G.; Barker, D.M.; et al. *A Description of the Advanced Research WRF Version 3*; National Center for Atmospheric Research: Boulder, CO, USA, 2019; no. 145; 550 p.
14. Shestakova, A.A.; Myslenkov, S.A.; Kuznetsova, A.M. Influence of Novaya Zemlya Bora on sea waves: Satellite measure-ments and numerical modeling. *Atmosphere* **2020**, *11*, 726. [CrossRef]
15. Cangialosi, J.P.; Latto, A.S.; Berg, R. Tropical cyclone report:hurricane irma (al112017), 30 August–12 September 2017. *Natl. Cent. Trop. Cyclone Rep.* **2018**, *111*. Available online: https://www.nhc.noaa.gov/data/tcr/AL112017_Irma.pdf (accessed on 13 June 2023).
16. Saha, S.; Moorthi, S.; Wu, X.; Wang, J.; Nadiga, S.; Tripp, P.; Behringer, D.; Hou, Y.-T.; Chuang, H.-Y.; Iredell, M.; et al. The NCEP Climate Forecast System Version 2. *J. Clim.* **2014**, *27*, 2185–2208. [CrossRef]
17. Hong, S.-Y.; Lim, J.-O.J. The WRF single–moment 6–class microphysics scheme (WSM6). *J. Korean Meteor. Soc.* **2006**, *42*, 129–151.
18. Iacono, M.J.; Delamere, J.S.; Mlawer, E.J.; Shephard, M.W.; Clough, S.A.; Collins, W.D. Radiative forcing by long-lived greenhouse gases: Calculations with the AER radiative transfer models. *J. Geophys. Res. Atmos.* **2008**, *113*, D13103. [CrossRef]
19. Jiménez, P.A.; Dudhia, J.; González-Rouco, J.F.; Navarro, J.; Montávez, J.P.; García-Bustamante, E. A Revised Scheme for the WRF Surface Layer Formulation. *Mon. Weather. Rev.* **2012**, *140*, 898–918. [CrossRef]
20. Hong, S.-Y.; Noh, Y.; Dudhia, J. A New Vertical Diffusion Package with an Explicit Treatment of Entrainment Processes. *Mon. Weather. Rev.* **2006**, *134*, 2318–2341. [CrossRef]
21. Zhang, C.; Wang, Y.; Hamilton, K. Improved Representation of Boundary Layer Clouds over the Southeast Pacific in ARW-WRF Using a Modified Tiedtke Cumulus Parameterization Scheme. *Mon. Weather. Rev.* **2011**, *139*, 3489–3513. [CrossRef]
22. Dudhia, J. A multi-layer soil temperature model for MM5. 1996. In Proceedings of the Sixth PSU/NCAR Mesoscale Model Users' Workshop, Boulder, Colorado, 22–24 July 1996.
23. Bryan, G.H.; Worsnop, R.P.; Lundquist, J.K.; Zhang, J.A. A Simple Method for Simulating Wind Profiles in the Boundary Layer of Tropical Cyclones. *Bound.-Layer Meteorol.* **2017**, *162*, 475–502. [CrossRef]
24. Chen, X. How Do Planetary Boundary Layer Schemes Perform in Hurricane Conditions: A Comparison With Large-Eddy Simulations. *J. Adv. Model. Earth Syst.* **2022**, *14*, e2022MS003088. [CrossRef]
25. Hong, S.Y.; Pan, H.L. Nonlocal boundary layer vertical diffusion in a medium-range forecast model. *Mon. Weather. Rev.* **1996**, *124*, 2322–2339. [CrossRef]
26. Biswas, M.K.; Abarca, S.; Bernardet, L.; Ginis, I.; Grell, E.; Iacono, M.; Kalina, E.; Liu, B.; Liu, Q.; Marchok, T.; et al. Hurricane Weather Research and Forecasting (HWRF) Model: 2018 Scientific Documentation. *Dev. Testbed Cent.* **2018**, *112*. Available online: https://opensky.ucar.edu/islandora/object/technotes:563 (accessed on 13 June 2023).
27. Nakanishi, M.; Niino, H. An improved Mellor–Yamada level 3 model: Its numerical stability and application to a regional pre-diction of advecting fog. *Bound. Layer Meteor.* **2006**, *119*, 397–407. [CrossRef]
28. Olson, J.B.; Smirnova, T.; Kenyon, J.S.; Turner, D.D.; Brown, J.M.; Zheng, W.; Green, B.W. A Description of the MYNN Surface-Layer Scheme. *NOAA Technol. Memo. OAR GSL-67* **2021**, *26*, 1–26. [CrossRef]
29. Mirocha, J.D.; Lundquist, J.; Kosović, B. Implementation of a Nonlinear Subfilter Turbulence Stress Model for Large-Eddy Simulation in the Advanced Research WRF Model. *Mon. Weather. Rev.* **2010**, *138*, 4212–4228. [CrossRef]
30. Kuznetsova, A.; Baydakov, G.; Sergeev, D.; Troitskaya, Y. High resolution waves and weather forecasts using adapted WAVE-WATCH III and WRF models. *J. Phys. Conf. Ser.* **2019**, *1163*, 1012031. [CrossRef]
31. Simon, J.S.; Zhou, B.; Mirocha, J.D.; Chow, F.K. Explicit Filtering and Reconstruction to Reduce Grid Dependence in Convective Boundary Layer Simulations Using WRF-LES. *Mon. Weather. Rev.* **2019**, *147*, 1805–1821. [CrossRef]
32. Kessler, E. *On the Distribution and Continuity of Water Substance in Atmoshperic Circulations*; American Meteorological Society: Boston, MA, USA, 1969; Volume 32, pp. 1–84.
33. Kain, J.S. The Kain–Fritsch convective parameterization: An update. *J. Appl. Meteor.* **2004**, *43*, 170–181. [CrossRef]

34. Mukul Tewari, N.C.A.R.; Tewari, M.; Chen, F.; Wang, W.; Dudhia, J.; LeMone, M.; Mitchell, K.; Ek, M.; Gayno, G.; Wegiel, J.; et al. Implementation and verification of the unified NOAH land surface model in the WRF model (Formerly Paper Number 17.5). In Proceedings of the 20th Conference on Weather Analysis and Forecasting/16th Conference on Numerical Weather Pre-Diction, Seattle, WA, USA, 10–15 January 2014; Volume 14.
35. Collins, W.; Rasch, P.; Boville, B.; McCaa, J.; Williamson, D.; Kiehl, J.; Briegleb, B.; Bitz, C.; Lin, S.-J.; Zhang, M.; et al. Description of the NCAR Community Atmosphere Model (CAM 3.0). *NCAR Tech. Note NCAR/TN-464+ STR* **2004**, *226*, 1326–1334.
36. Pollard, R.T.; Rhines, P.B.; Thompson, R.O.R.Y. The deepening of the wind-Mixed layer. *Geophys. Fluid Dyn.* **1973**, *4*, 381–404. [CrossRef]
37. Donelan, M.A. On the Decrease of the Oceanic Drag Coefficient in High Winds. *J. Geophys. Res. Ocean.* **2018**, *123*, 1485–1501. [CrossRef]
38. Hinze, J.O. *Turbulence: An Introduction to Its Mechanism and Theory*, 1st ed.; McGraw-Hill: New York, NY, USA, 1959; p. 586.
39. Poplavsky, E.; Rusakov, N.; Ermakova, O.; Sergeev, D.; Troitskaya, Y. Towards an Algorithm for Retrieval of the Parameters of the Marine Atmospheric Boundary Layer at High Wind Speeds Using Collocated Aircraft and Satellite Remote Sensing. *J. Mar. Sci. Eng.* **2022**, *10*, 1136. [CrossRef]
40. Aragon, L.G.B.; Pura, A.G. Analysis of the displacement error of the WRF-ARW model in predicting tropical cyclone tracks over the Philippines. *Meteorol. Appl.* **2016**, *23*, 401–408. [CrossRef]
41. Ermakova, O.; Rusakov, N.; Poplavsky, E.; Sergeev, D.; Troitskaya, Y. Friction Velocity and Aerodynamic Drag Coefficient Retrieval from Sentinel-1 IW Cross-Polarization C-SAR Images under Hurricane Conditions. *Remote. Sens.* **2023**, *15*, 1985. [CrossRef]
42. Holthuijsen, L.H.; Powell, M.; Pietrzak, J.D. Wind and waves in extreme hurricanes. *J. Geophys. Res. Ocean.* **2012**, *117*, C09003. [CrossRef]